Genetic analysis of the contribution of the proprotein convertases to the *in vivo* regulation of FGF23

Running title: Proprotein convertases in the regulation of FGF23

Omar Al Rifai[1,2], Delia Susan-Resiga[3], Rachid Essalmani[3], John W.M. Creemers[4], Nabil G. Seidah[3] and Mathieu Ferron[1,2,5,6]#

[1] Unité de recherche en physiologie moléculaire, Institut de Recherches Cliniques de Montréal, Montréal, Québec H2W 1R7, Canada
[2] Programme de biologie moléculaire, Université de Montréal, Québec H3T 3J7, Canada
[3] Unité de recherche en biochimie neuroendocrinienne, Institut de Recherches Cliniques de Montréal, Montréal, Québec H2W 1R7, Canada
[4] Department of Human Genetics, KU Leuven, Herestraat 49, B-3000 Leuven, Belgium
[5] Département de Médecine, Université de Montréal, Québec H3T 3J7, Canada
[6] Division of Experimental Medicine, McGill University, Montréal, Québec H3A 1A3, Canada

Omar.alrifai@ircm.qc.ca; Delia.Susan-Resiga@ircm.qc.ca; Rachid.Essalmani@ircm.qc.ca; john.creemers@kuleuven.be; Nabil.Seidah@ircm.qc.ca; mathieu.ferron@ircm.qc.ca

Correspondence to:

Mathieu Ferron, PhD
Institut de Recherches Cliniques de Montréal
110 Ave. des Pins O.
Montréal, QC,
H2W 1R7, Canada
Phone: 514-987-5754
Fax: 514-987-5649
Email: mathieu.ferron@ircm.qc.ca

Author contributions: MF, DSR and OAR conceived and planned the experiments. OAR and DSR carried out the experiments. OAR and MF analyzed the data. RE, JWMC and NGS provided critical mouse lines. OAR and MF wrote the manuscript with input from all authors.

Keywords

FGF23, endoproteolysis, proprotein convertases, Furin, PC5, PACE4, phosphate

ABSTRACT

Fibroblast growth factor 23 (FGF23) is a hormone secreted from terminally differentiated osteoblasts and by osteocytes that inhibits phosphate reabsorption by kidney proximal tubules. The full-length (i.e., intact) protein mediates FGF23 endocrine functions, while endoproteolytic cleavage at a consensus cleavage sequence for the proprotein convertases (PCs) inactivates it. Two PCs, furin and PC5, were shown to cleave FGF23 *in vitro* at $RHTR_{179}\downarrow$, but those involved in FGF23 processing *in vivo* are not defined. Here, we assessed FGF23 processing and phosphate metabolism in mice lacking either or both furin and PC5 in the osteoblastic lineage and/or in hematopoietic cells, and in mice lacking the paired basic amino acid-cleaving enzyme 4 (PACE4) in all tissues. Our results showed that furin inactivation in osteoblasts and osteocytes results in a 25% increase in circulating intact FGF23, without any significant impact on serum phosphate levels, whether mice are maintained on a normal or a low phosphate diet. Under conditions of iron deficiency, FGF23 processing is impaired in mice lacking furin in osteoblasts and osteocytes, while it is normally processed in control mice. In contrast, FGF23 is normally processed following erythropoietin or IL-1β injections in mice lacking furin or both furin and PC5, and in PACE4-deficient mice. Altogether, these studies suggest that furin is only partially responsible for FGF23 cleavage under certain conditions *in vivo*. The processing of FGF23 may therefore involve the redundant action of multiple PCs or of other peptidases in osteoblasts, osteocytes and hematopoietic cells.

INTRODUCTION

Fibroblast growth factor 23 (FGF23) is a bone-derived hormone (i.e., osteokine) secreted by terminally differentiated cells of the osteoblast lineage, including osteoblasts and osteocytes. It plays a fundamental role in phosphate and vitamin D metabolism in particular through a direct action on the kidney [1,2]. In this tissue, its signaling is mediated through interaction with the FGF receptor 1 (FGFR1) and its co-receptor α-klotho [3]. FGFR1/α-klotho signaling in the kidney proximal tubule suppresses the transcription of *Slc34a1* and *Slc34a3*, the genes encoding for the sodium phosphate co-transporters NaPi2A and NaPi2C, resulting in increased urinary phosphate excretion and decreased serum phosphate levels. In addition, FGF23 reduces the 1,25-dihydroxyvitamin D_3 (calcitriol) level by decreasing expression of *Cyp27b1* which encodes the 25-hydroxyvitamin D-1 alpha hydroxylase and increasing expression of *Cyp24a1* which encodes the 1,25-dihydroxyvitamin D_3 24-hydroxylase [4-7]. These endocrine functions are mediated through full-length "intact" FGF23 (amino acids [aa] 25-251). Endoproteolytic cleavage of FGF23 at the basic motif $\underline{\mathbf{R}}_{176}HT\underline{\mathbf{R}}_{179}$↓SA, a consensus P1 and P4 arginine (Arg) cleavage site for proprotein convertases (PCs), inactivates FGF23 by releasing N-terminal (aa 25-179) and C-terminal (aa 180-251) fragments.

The circulating level of intact FGF23 is tightly regulated in part through various post-translational modifications of amino acids surrounding the PC cleavage site. The *O*-glycosylation of threonine 178 (T_{178}) by the *N*-acetylgalactosaminyltransferase 3 (GalNAc-T3) inhibits FGF23 processing [8-10]. FGF23 *O*-glycosylation is in turn reduced when the serine 180 (S_{180}) is phosphorylated by Fam20c, a kinase residing in the Golgi

82 [11]. Impaired FGF23 glycosylation caused by a defective GalNAc-T3 or mutation in FGF23
83 glycosylation sites cause an increase in FGF23 processing and subsequent decrease in
84 circulating intact FGF23 levels. These molecular defects lead to familial tumoral calcinosis
85 (FTC), a human disease characterized by hyperphosphatemia and heterotopic
86 calcification [8-10]. On the other hand, mutations in the FGF23 cleavage site and in the X-
87 linked phosphate-regulating neutral endopeptidase (PHEX) respectively cause
88 autosomal dominant hypophosphatemic rickets (ADHR) and X-linked hypophosphatemic
89 rickets (XLH). Patients with ADHR and XLH develop hypophosphatemia and
90 osteomalacia due to the increased level of active intact FGF23 [12,13]. Iron deficiency,
91 erythropoietin treatment or interleukin-1 beta (IL-1β) were shown to stimulate FGF23
92 production by osteocytes and bone marrow hematopoietic cells [14-19]. However, this
93 increase in FGF23 production only results in the accumulation of intact FGF23 levels and
94 hypophosphatemia in ADHR patients or in mice with an ADHR-like mutation in *Fgf23*. In
95 wildtype animals or healthy subjects, the same stimuli result in increased circulating levels
96 of cleaved FGF23, revealing the importance of endoproteolysis by PC for the regulation
97 of this hormone.
98
99 The proprotein convertases furin and PC5 were shown to cleave FGF23 *in vitro* [20], while
100 inactivation of *FURIN* in the human osteosarcomas U2-OS cell line impaired the cleavage
101 of ectopically expressed human FGF23 [11]. Nevertheless, despite the implication of FGF23
102 cleavage in several human diseases, the identity of the enzyme(s) responsible for FGF23
103 endoproteolysis *in vivo* remains undetermined. In the present study we assessed the
104 requirement of furin and PC5 for FGF23 processing and phosphate metabolism *in vivo*.

105 We showed that furin inactivation in the osteoblastic lineage results in a modest increase
106 in intact FGF23 under normal or low phosphate diet, while it impairs FGF23 cleavage in
107 conditions of iron deficiency. We also show that furin, PC5 and PACE4, another PC
108 expressed in osteoblasts, which can cleave FGF23 *in vitro*, are dispensable for the
109 cleavage and inactivation of FGF23 *in vivo* following treatment with erythropoietin or IL-
110 1β. Together, our data suggest that furin is involved in FGF23 cleavage *in vivo*, but that
111 multiple other PC(s) are also implicated in this process.
112
113

114 **RESULTS**

115

116 **Furin inactivation in osteoblasts and osteocytes partially impairs FGF23 cleavage,**
117 **but decreases phosphate excretion**

118 To investigate the role of furin in the regulation of FGF23 processing *in vivo*, we generated
119 mice in which the *Furin* gene was specifically inactivated in osteoblasts and osteocytes
120 (i.e., *Furin*^{osb}*-/-*) by breeding *Furin*$^{fl/fl}$ mice with *hOCN-Cre* transgenic animals which
121 express the Cre recombinase under the control of human osteocalcin promoter [21]. We
122 previously reported that the *Furin* gene was efficiently and specifically inactivated in
123 osteoblasts and bones in these mice [22]. When fed a normal chow diet containing ~0.7%
124 inorganic phosphate (Pi), 4-month-old *Furin*^{osb}*-/-* female mice displayed a significant 25%
125 rise in circulating intact FGF23 (Figure 1A). This moderate increase did not significantly
126 alter the expression of *Slc34a1*, *Slc34a3*, *Cyp27b1* or *Cyp24a1* (Figure 1B). Accordingly,
127 these mice maintained normal serum phosphate levels and bone histology did not reveal
128 presence of osteomalacia (Figure 1C and D).

129

130 Serum phosphate level is a potent regulator of FGF23 and previous studies have shown
131 that in mice fed a low-phosphate synthetic diet the serum level of intact FGF23 is reduced,
132 while the processed fraction is increased, presumably due to the action of one or several
133 PCs [23-25]. We therefore next assessed if severe hypophosphatemia could be induced in
134 *Furin*^{osb}*-/-* mice under low phosphate dietary intake. Feeding control and *Furin*^{osb}*-/-* mice
135 normal phosphate diet (i.e., 0.6% Pi) or low-phosphate diet (0.02% Pi) for one week did
136 not affect body weight or kidney weight (Figure 1E and F). As expected, serum

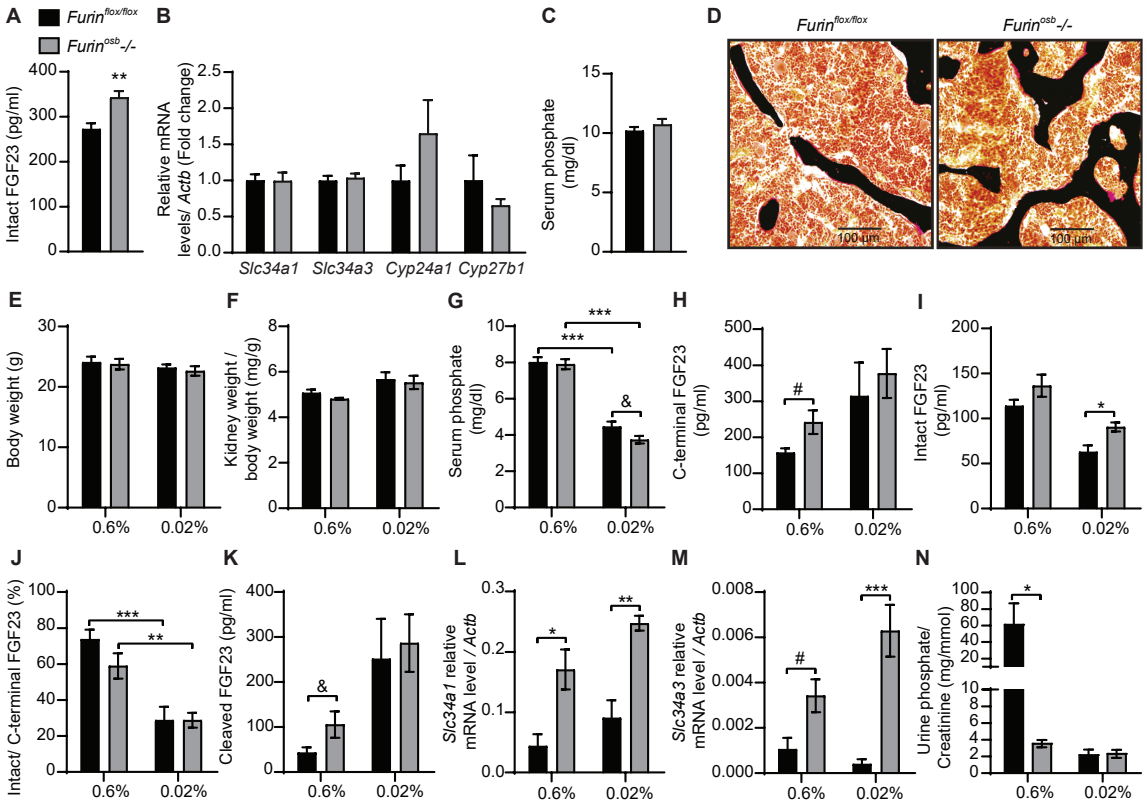

Figure 1: Increased FGF23 level and reduced phosphate excretion in *Furin^{osb}*-/- mice. FGF23 and phosphate levels in in 4-month-old *Furin$^{flox/flox}$* (n=6) and *Furin^{osb}*-/- (n=6) mice fed on normal chow diet **(A-D)**. Intact FGF23 levels in plasma **(A)**. FGF23 target genes expression in kidney **(B)**. Serum phosphate level **(C)**. Von Kossa / van Gieson staining on vertebrae sections **(D)**. FGF23 and phosphate parameters in 6-months-old *Furin$^{flox/flox}$* (n=6) and *Furin^{osb}*-/- (n=6-7) mice fed a normal phosphate diet (0.6%) or a low phosphate diet (0.02%) for one week **(E-N)**. Body weight **(E)**. Kidney weight normalize to body weight **(F)**. Serum phosphate levels **(G)**. Plasma level of C-terminal FGF23 **(H)**, intact FGF23 **(I)**, percentage (%) of intact over C-terminal FGF23 **(J)** and cleaved FGF23 levels **(K)** calculated as (C-terminal FGF23) - (intact FGF23). Expression level in kidney of the sodium phosphate cotransporter *Slc34a1* **(L)** and *Slc34a3* **(M).** **(N)** Urine phosphate measurements normalized to creatinine. Results represent the mean ± SEM. *P < 0.05, **P < 0.01, and ***P < 0.001, by 2-way ANOVA with Bonferroni's multiple comparisons test or by Student's t-test (A, C, G, H, K, and M) #: P<0.05; # #: P<0.01, # # #: P<0.001 &: 0.05<P<0.1.

phosphate level decreased significantly in both control and *Furin^{osb}*-/- mice fed the low phosphate diet (Figure 1G). Under the same conditions, *Furin^{osb}*-/- mice tend to have a lower serum phosphate level compared to control mice, although this did not reach statistical significance. *Furin^{osb}*-/- mice on normal diet had >25% increase in intact and C-terminal (total) FGF23, while maintaining normal intact/C-terminal FGF23 ratio compared to control littermates (Figure 1H-J). Under low phosphate diet circulating intact FGF23

156 was reduced in control mice but remains significantly higher in *Furin*^{osb}*-/-* mice (Figure 1I).
157 Yet, the ratio of intact over C-terminal FGF23 was decreased in both control and *Furin*^{osb}-
158 /- mice under low phosphate diet (Figure 1J). Moreover, the amount of cleaved FGF23
159 (i.e., C-terminal FGF23 minus intact FGF23) was increased regardless of the genotype
160 on low phosphate diet, suggesting efficient cleavage of FGF23 even in absence of furin
161 (Figure 1K). Surprisingly, when fed these synthetic diets, *Furin*^{osb}*-/-* mice displayed an
162 increased expression in the kidney of the sodium phosphate transporter genes *Slc34a1*
163 and *Slc34a3* compared to control group, independently of the level of phosphate in the
164 diet (Figure 1L and M). In addition, *Furin*^{osb}*-/-* mice on normal phosphate diet showed a
165 decrease in urinary phosphate compared to control littermate (Figure 1N). Challenging
166 the mice for one week on the low phosphate diet reduced urinary phosphate in control
167 mice as expected, but not in *Furin*^{osb}*-/-* mice, as these mice maintained the low urinary
168 phosphate observed on normal phosphate diet (Figure 1N). Together these results show
169 that under physiological conditions or in conditions of decreased phosphate intake,
170 inactivation of *Furin* in the osteoblast lineage modestly impacted FGF23 processing. They
171 also suggest that furin may influence phosphate excretion through FGF23-independent
172 mechanisms.
173

174 **Impact of iron deficiency on FGF23 processing and phosphate metabolism in**
175 **absence of furin in osteoblasts and osteocytes**

176 It was previously reported that mice carrying an ADHR mutation (R176Q, i.e., loss of P4
177 Arg in the motif **R**$_{176}$HT**R**$_{179}$↓SA) in the *Fgf23* gene did not develop hypophosphatemia
178 unless they were fed a low-iron diet [15]. Therefore, iron-deficiency was induced in control

179 and *Furin*^{osb}*-/-* mice by feeding them a low-iron diet in combination with repeated tail
180 bleedings (i.e., ~70 μl every other week) for 14 weeks, before assessing the impact on
181 FGF23 and phosphate metabolism. Mice of both genotypes maintained normal growth
182 curves in these conditions as compared to mice fed the control chow diet (Figure 2A).

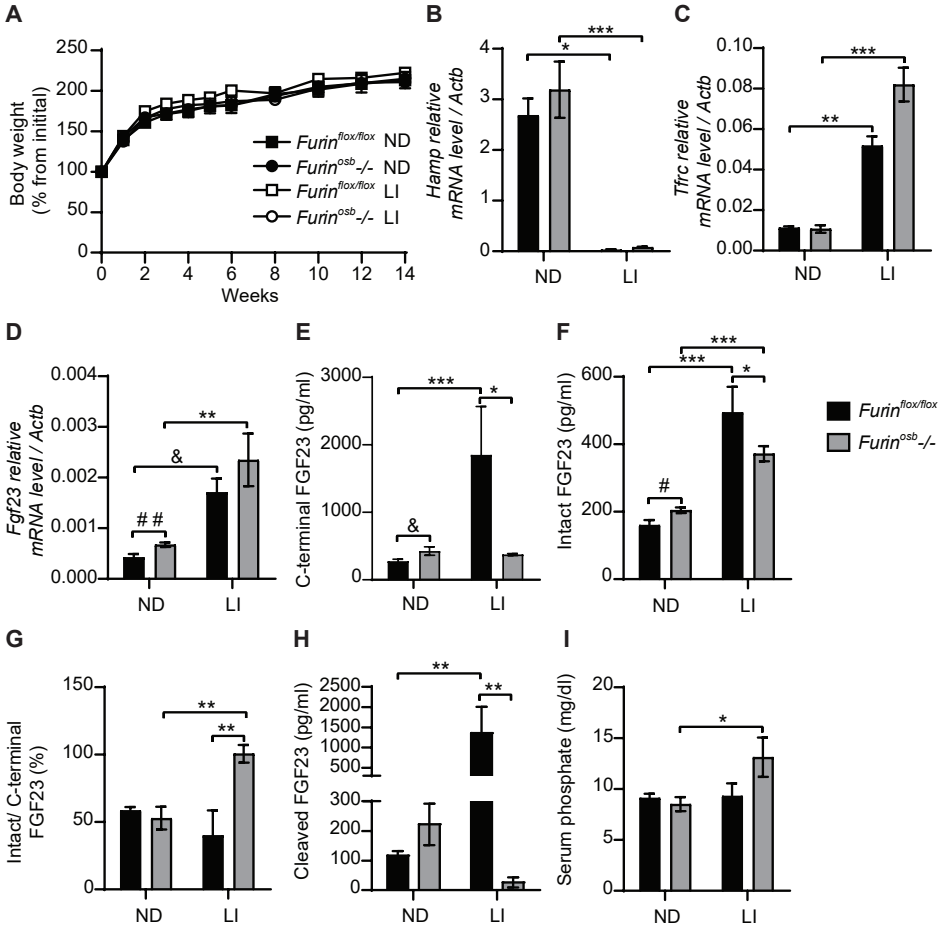

183 **Figure 2: Impaired FGF23 processing in *Furin*^{osb}*-/-* mice following iron restriction.** *Furin*$^{flox/flox}$ (n=3-5)
184 and *Furin*^{osb}*-/-* (n=7-8) 21-day-old mice were fed normal chow diet (ND) or a low iron diet (LI) for 14 weeks.
185 **(A)** Body weight growth curve presented as percentage of initial body weight. **(B-C)** Expression of iron-
186 regulated genes in liver. Hepcidin (*Hamp*) expression **(B)**. Transferrin receptor (*Tfrc*) expression **(C). (D)**
187 *Fgf23* expression in long bone. **(E-H**) Plasma level of C-terminal FGF23 **(E)**, intact FGF23 **(F)**, percentage
188 (%) of intact over C-terminal FGF23 **(G)** and cleaved FGF23 levels **(H)**, calculated as (C-terminal FGF23)
189 - (intact FGF23). **(I)** Serum phosphate levels. Results represent the mean ± SEM. **P* < 0.05, ***P* < 0.01,
190 and ****P* < 0.001, by 2-way ANOVA with Bonferroni's multiple comparisons test or by Student's t-test (D
191 and E) #: *P*<0.05; # #: *P*<0.01, # # #: *P*<0.001 &: 0.05<*P*<0.1.
192
193 However, challenged mice developed iron deficiency as reflected by the decrease in
194 hepcidin (*Hamp*) expression and the increase in transferrin receptor (*Tfrc*) expression in

195 liver (Figure 2B-C). As expected from a previous study [15], iron deficient control and
196 *Furin*^{osb}*-/-* mice displayed an increase in *Fgf23* gene expression in bone (Figure 2D).
197 However, iron-deficiency resulted in increased C-terminal FGF23 only in control mice,
198 although both genotypes showed an increase in intact FGF23 (Figure 2E-F). FGF23
199 processing appears to be totally impaired in *Furin*^{osb}*-/-* mice under conditions of iron
200 deficiency as these mice maintained a 1:1 ratio (i.e., 100%) of intact over C-terminal
201 FGF23 and very low level of cleaved FGF23 (Figure 2G-H). Yet, despite this near
202 complete inhibition in FGF23 processing, *Furin*^{osb}*-/-* mice displayed a paradoxical
203 increase in serum phosphate level compared to the control littermates under iron
204 deficiency (Figure 2I). Altogether these results suggest that furin is responsible for FGF23
205 processing under iron deficiency. However, under these conditions the absence of furin
206 in osteoblasts and osteocytes also results in a compensatory increase in serum
207 phosphate levels in an FGF23-independent manner.
208

209 **Normal FGF23 processing in absence of furin in osteoblasts and osteocytes**
210 **following rhEPO and IL-1β injections**

211 Anemia and inflammation may contribute to the onset of ADHR [16-19,26]. Erythropoietin and
212 interleukin 1 beta (IL-1β), which are increased in condition of anemia and inflammation
213 respectively, are two potent inducers of *Fgf23* at the transcriptional level [16-19,26,27]. In wild
214 type mice, most (i.e., >80%) of the circulating FGF23 is in its cleaved form following
215 recombinant human erythropoietin (rhEPO) or IL-1β injections, suggesting the action of
216 one or multiple PC in these particular conditions [16,17,19]. We therefore next tested the

impact of furin deficiency in osteoblasts and osteocytes on FGF23 processing 6 hours after a single injection of rhEPO or IL-1β.

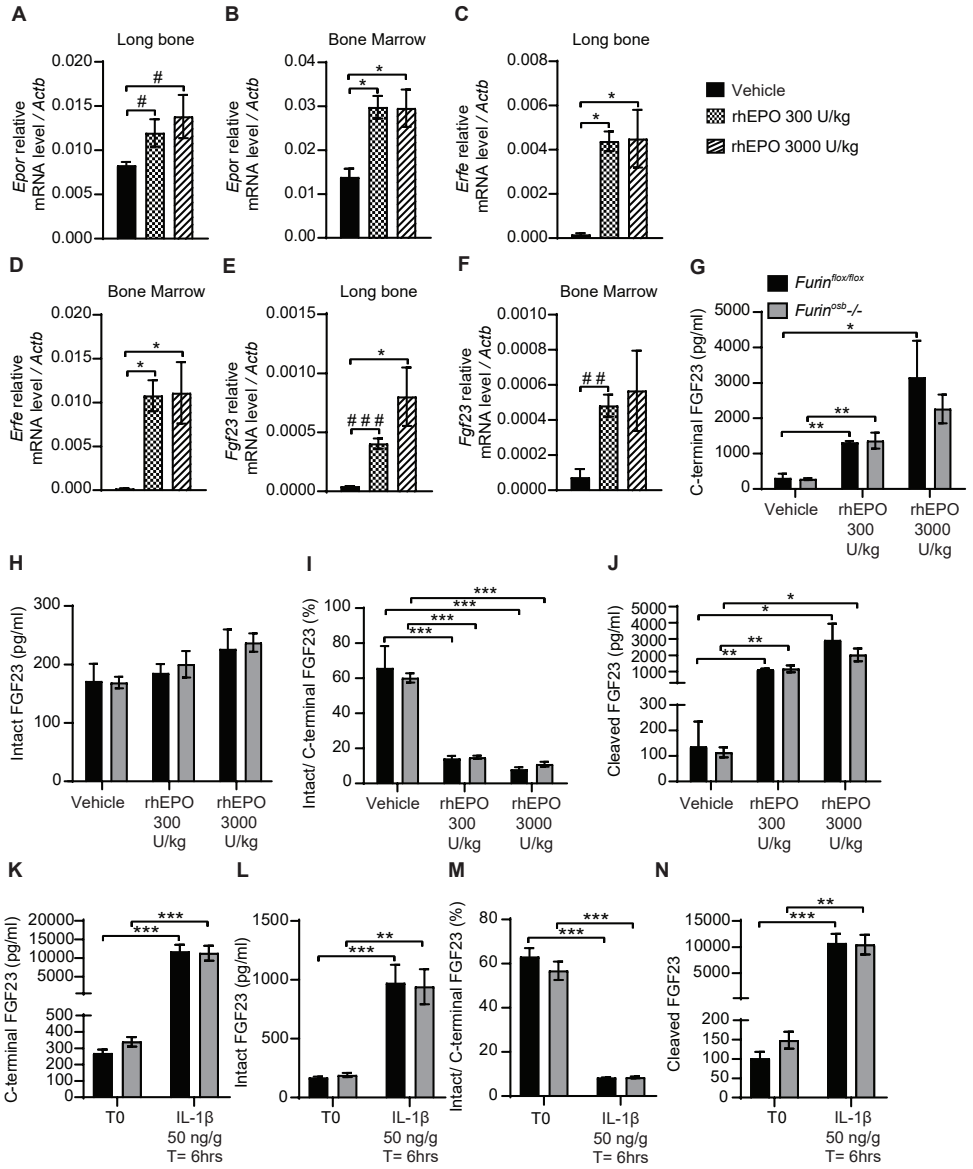

Figure 3: FGF23 is normally processed following erythropoietin and IL-1β injection in *Furin*^{osb}*-/-* mice. Genes expression in long bone **(A, B and E)** and bone marrow **(C, D and F)** of 2-month-old C57BL/6J mice 6 hours following the injection of vehicle (n=4), 300 U/kg (n=4) or 3000 U/kg (n=4) of recombinant human erythropoietin (rhEPO). Erythropoietin receptor (*Epor*) **(A and C)**, erythroferrone (*Erfe*) **(B and D)** and FGF23 (*Fgf23*) **(C and F)**. **(G-J)** Plasma FGF23 measurements in 4-month-old *Furin*$^{flox/flox}$ (n=3) and *Furin*^{osb}*-/-* (n=3) mice 6 hours following the injection of vehicle, 300 U/kg or 3000 U/kg of rhEPO. C-terminal FGF23 **(G)**, intact FGF23 **(H),** percentage (%) of intact over C-terminal FGF23 **(I)** and cleaved FGF23 levels **(J)**, calculated as (C-terminal FGF23) - (intact FGF23). **(K-N)** Plasma FGF23 measurements in 4-month-old *Furin*$^{flox/flox}$ (n=4) and *Furin*^{osb}*-/-* (n=4) mice before (T0) and 6 hours following the injection of 50 ng/g IL-1β (T=6hrs). C-terminal FGF23 **(K)**, intact FGF23 **(L),** percentage (%) of intact over C-terminal FGF23 **(M)** and cleaved FGF23 levels **(N)**. Results represent the mean ± SEM. *$P < 0.05$, **$P < 0.01$, and ***$P < 0.001$, by 1-way ANOVA **(A-F)** or 2-way ANOVA **(G-N)** with Bonferroni's multiple comparisons test, or by Student's t-test **(A and E)** #: $P<0.05$; # #: $P<0.01$, # # #: $P<0.001$ &: $0.05<P<0.1$.

232 Because of variation in the doses of rhEPO used in the literature to induce FGF23 in
233 rodents [17-19,26,27], we first confirmed that two relatively low doses of rhEPO (i.e., 300U/kg
234 and 3000U/kg) were sufficient to induce in bones and bone marrow of wild type C57BL/6J
235 mice the expression of two known EPO target genes, erythropoietin receptor (*Epor*) and
236 erythroferrone (*Erfe*) (Figure 3A-D). These two doses also robustly induced the
237 expression of *Fgf23* in both tissues in the same animals (Figure 3E-F). We next assessed
238 the effect of the same treatment in control and *Furin*^{osb}*-/-* mice. Circulating level of total
239 (C-terminal) FGF23 was increased in a dose dependent manner by rhEPO, while intact
240 FGF23 was modestly changed regardless of the genotype (Figure 3G-H). The ratio of
241 intact over C-terminal FGF23 level was robustly reduced by the same treatment (Figure
242 3I) and cleaved FGF23 was increased more than 10-fold by rhEPO in both control and
243 *Furin*^{osb}*-/-* mice (Figure 3J), suggesting that in this context, FGF23 is normally processed
244 even in absence of furin in osteoblasts and osteocytes.
245
246 In separate experiments, control and *Furin*^{osb}*-/-* mice were administered a single dose of
247 IL-1β (50ng/g), a treatment which was previously shown to induce *Fgf23* expression in
248 bone and to raise total FGF23 circulating level within a few hours [16]. Six hours after the
249 injection of IL-1β, the level of total (C-terminal) FGF23 increased by more than 30-fold,
250 while intact FGF23 increased by less than 10-fold, in both control and *Furin*^{osb}*-/-* mice
251 (Figure 3K-L). Following the IL-1β treatment and regardless of the mouse genotype, the
252 ratio of intact over C-terminal FGF23 level decreased from 60% to less than 10% (Figure
253 3M) and the plasma concentration of cleaved FGF23 increased more than 10 times
254 (Figure 3N). Together, these data show that FGF23 is efficiently processed in absence of

255 furin in osteoblasts and osteocytes following rhEPO or IL-1β injections, likely to the
256 contribution of other processing enzymes.
257
258 **FGF23 is processed in mice lacking furin in osteoblasts, osteocytes and**
259 **hematopoietic cells following rhEPO injections**
260 The data presented above suggest that under normal conditions furin is partially
261 responsible for FGF23 cleavage, but that in the context of iron deficiency, osteocytes-
262 derived furin may be a major contributor to the processing of FGF23. In contrast, FGF23
263 was normally processed following rhEPO or IL-1β injection in *Furin*^{osb}*-/-* mice. Osteoblasts
264 and osteocytes are the main source of circulating FGF23 in normal conditions [26,28], but
265 bone marrow hematopoietic cells contribute to approximately 40% of circulating FGF23
266 following rhEPO treatment [26]. Therefore, in *Furin*^{osb}*-/-* mice, bone marrow hematopoietic
267 cells could be a significant source of cleaved FGF23 following rhEPO injections, thereby
268 masking the impact of furin inactivation in osteoblasts and osteocytes. To test this
269 possibility, we generated mice lacking furin in all hematopoietic cells by breeding
270 *Furin*$^{flox/flox}$ mice with *Vav1-Cre* to generate *Furin*$^{flox/flox}$*; Vav1-Cre* mice (*Furin*^{BM}*-/-*). *Vav1-*
271 *Cre* transgenic animals expresses the Cre recombinase under the control of the *Vav1*
272 promoter, allowing the efficient deletion of furin in fetal and adult hematopoietic stem cells
273 (HSC) [29] and hence in all hematopoietic cells. To address any potential redundancy
274 between osteocytes and hematopoietic cells in the cleavage of FGF23, we also generated
275 mice lacking *Furin* in both cell types, i.e., *Furin*$^{flox/flox}$*;* hOCN-Cre*;* Vav1-Cre mice
276 (*Furin*$^{osb;BM}$*-/-*). Furin deficiency in T cells impairs the function of regulatory and effector T
277 cells, causing at around 6 month of age severe inflammatory bowel disease, weight loss,

278 ruffled hair and hunched appearance [30]. Confirming efficient inactivation of *Furin* in
279 hematopoietic cells, these defects were also observed in our *Furin*^{BM}*-/-* mice between 4
280 and 6 months of age (data not shown). Hence, in the following experiments all mice were
281 8 weeks of age, a time point at which the *Furin*^{BM}*-/-* mice are still healthy.

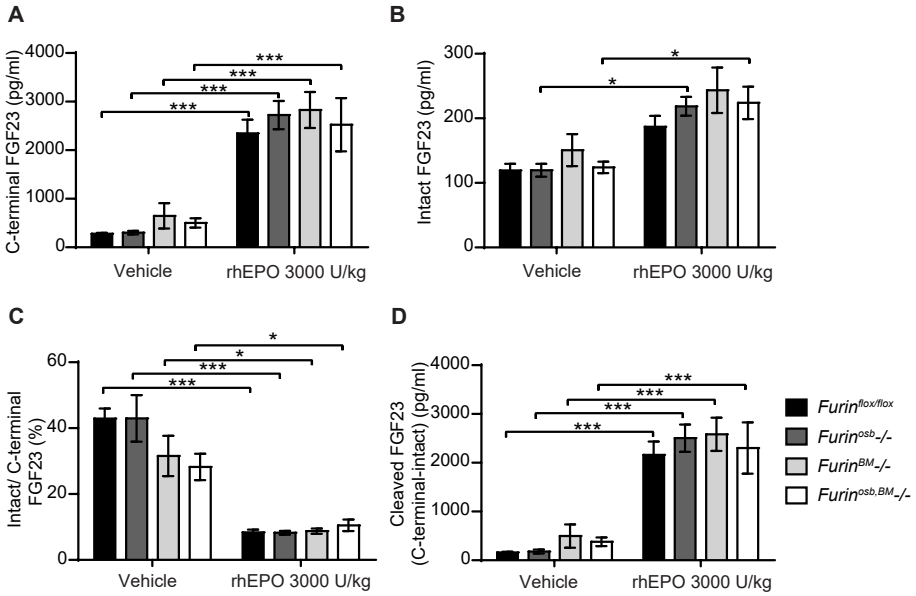

282 **Figure 4: *Furin* inactivation in osteoblasts, osteocytes and hematopoietic cells did not impair FGF23**
283 **processing following erythropoietin injection.** Plasma FGF23 measurements in 8-week-old *Furin*$^{flox/flox}$
284 (n=7), *Furin*^{osb}*-/-* (n=5), *Furin*^{osb}*-/-* (n=5) and *Furin*$^{osb;BM}$*-/-* (n=6) mice 6 hours following injection of vehicle
285 or 3000 U/kg of recombinant human erythropoietin (rhEPO): C-terminal FGF23 **(A)**, intact FGF23 **(B)**,
286 percentage (%) of intact over C-terminal FGF23 **(C)** and cleaved FGF23 levels **(D)**, calculated as (C-
287 terminal FGF23) - (intact FGF23). Results represent the mean ± SEM. **P* < 0.05 and ****P* < 0.001, by 2-
288 way ANOVA with Bonferroni's multiple comparisons test.
289

290 A single injection of rhEPO (3000U/kg) increased total (C-terminal) FGF23 by 20-30 fold
291 and intact FGF23 by about 2 fold in control (*Furin*$^{flox/flox}$), *Furin*^{osb}*-/-*, *Furin*^{BM}*-/-* and
292 *Furin*$^{osb;BM}$*-/-* mice (Figure 4A-B). The same treatment also reduced the ratio of intact over
293 C-terminal FGF23 from 40% to <10%, while cleaved FGF23 level increased to the same
294 extent (>10 fold) in all genotypes (Figure 4C-D). Together these results show that FGF23
295 is still processed in absence of furin in osteoblasts/osteocytes and bone marrow

296 hematopoietic cells following rhEPO injections, suggesting that additional PCs may
297 redundantly cleave FGF23 in these cells *in vivo*.

298
299 **Figure 5: Multiple proprotein**
300 **convertases can process FGF23**
301 **in mammalian cells. (A)** Western
302 blot analysis of the secretion media
303 (SM) from CHO-K1 cells transfected
304 with V5 tagged human FGF23
305 (hFGF23-V5) and cultured in the
306 absence (-) or presence (+) of PC
307 inhibitors, decanoyl-RVKR-CMK
308 (RVKR) (50 μM) or hexa-D-arginine
309 (D6R) (20 μM). **(B)** Western blot
310 analysis of the secretion media (SM)
311 from CHO furin-deficient FD11 cells
312 co-transfected with V5 tagged
313 human FGF23 (hFGF23-V5) and
314 proprotein convertase Furin, PC5A,
315 PC5B, PACE4 or PC7. Intact and
316 processed C-terminal (CT) FGF23
317 forms are detected with V5 antibody.
318

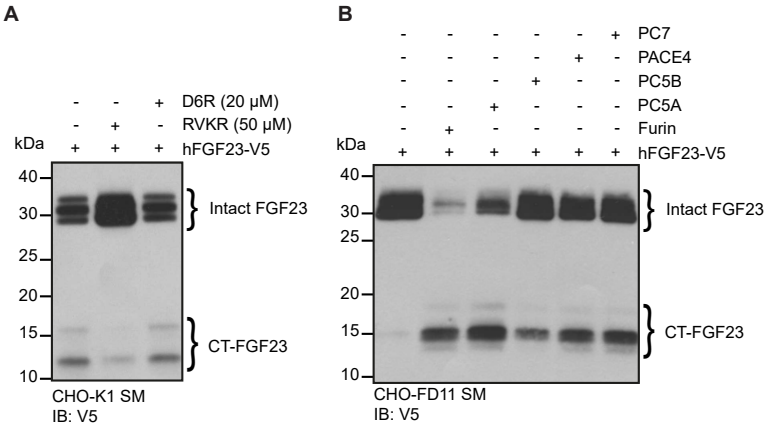

319 **Several PCs can process FGF23 in cell culture**

320 Our data suggests that in some conditions (e.g., low phosphate diet, rhEPO injection or
321 IL-1β injection), more than one PC may be involved in FGF23 cleavage. In order to identify
322 which additional PC(s) might be involved in FGF23 processing, we tested FGF23
323 processing in cell lines expressing or not furin. In Chinese hamster ovary (CHO-K1) cells,
324 which endogenously express furin [31], ectopically transfected human FGF23 is secreted
325 and partially processed (Figure 5A). In the same cells, cleavage of FGF23 was inhibited
326 by decanoyl-RVKR-CMK (RVKR) a pan-PC cell-permeable inhibitor, but not by hexa-D-
327 arginine (D6R), a cell-surface PC inhibitor (Figure 5A), suggesting that cleavage of
328 FGF23 occurs before it is secreted in an intracellular secretory compartment, likely the
329 trans-Golgi network [32]. In addition, FGF23 was not cleaved in CHO-FD11 cells, which do
330 not endogenously express furin [31], and co-transfection with a furin expressing vector was

331 sufficient to restore efficient cleavage (Figure 5B, first two lanes). We next tested the
332 capacity of other PCs, i.e., PC5A, PC5B, PACE4 and PC7 [33], to process FGF23 in the
333 same cells. Interestingly in this assay, PC5A was almost as efficient as furin in processing
334 FGF23. Moreover, PC5B, PACE4 and PCSK7 were also found to process FGF23
335 although to a lower extent than furin and PC5A (Figure 5B). Altogether, these results
336 indicate that in addition to furin, several other PCs have the capacity to process FGF23
337 in a mammalian cell line.
338

339 **Genetic ablation of PC5 and furin in osteoblasts and osteocytes does not impair**
340 **FGF23 processing**

341 Our data shows that PC5A and PC5B, which are both encoded by *Pcsk5* [33], can cleave
342 FGF23 in cell culture, and PC5A is expressed in differentiated osteoblasts and in
343 osteocytes [20,22]. We therefore next generated mice in which *Pcsk5* was inactivated
344 specifically in osteoblasts and osteocytes by breeding *Pcsk5*$^{fl/fl}$ mice [34] with hOCN-Cre
345 transgenic animals. When fed a normal chow diet, control (*Pcsk5*$^{fl/fl}$) and *Pcsk5*^{osb}*-/-* mice
346 displayed similar circulating level of intact FGF23 and serum phosphate (Figure 6A-B).
347 Von Kossa/van Gieson staining on non-decalcified bone sections did not reveal any sign
348 of osteomalacia in these mice (Figure 6C). These analyses suggest that PC5 in the
349 osteoblast lineage is dispensable for the regulation of FGF23 and phosphate levels *in*
350 *vivo*.

To test if PC5 and furin redundantly cleave FGF23 *in vivo*, we next generated mice lacking both furin and PC5 specifically in osteoblasts and osteocytes (i.e., *Furin*$^{flox/flox}$; *Pcsk5*$^{flox/flox}$; hOCN-Cre or *Furin;Pcsk5*^{osb}*-/-* mice). Similar to the single inactivation of furin in the same cells, osteoblast and osteocytes-specific inactivation of furin and PC5 resulted in a modest increase in circulating intact FGF23 when mice were fed normal or low phosphate diet (Figure 6D). A single injection of rhEPO (300U/kg) increased total (C-terminal) FGF23 by almost 10-fold and intact FGF23 by 25% in both control and *Furin;Pcsk5*^{osb}*-/-* mice (Figure 6E-F). Following the same treatment, intact over C-terminal ratio decreased by approximately 80%, while cleaved FGF23 increased more than 10-fold, regardless of the

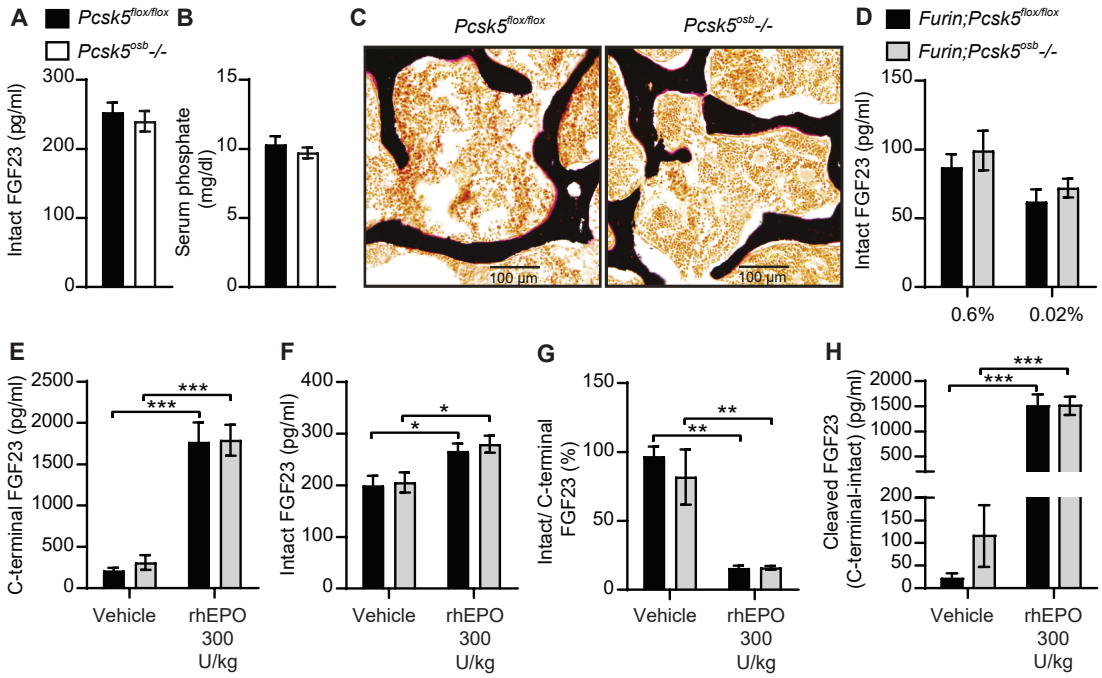

Figure 6: Genetic ablation of PC5 alone or in combination with Furin does not impair FGF23 processing *in vivo*. Plasma intact FGF23 **(A)** and serum phosphate levels **(B)** in 4-month-old *Pcsk5*$^{flox/flox}$ (n=6) and *Pcsk5*^{osb}*-/-* (n=7) mice fed a normal chow diet. **(C)** Von Kossa / van Gieson staining of vertebrae sections of *Pcsk5*$^{flox/flox}$ and *Pcsk5*^{osb}*-/-*. **(D)** Plasma intact FGF23 in 6-month-old *Furin;Pcsk5*$^{flox/flox}$ (n=7-8) and *Furin;Pcsk5*^{osb}*-/-* (n=8) fed a normal phosphate diet (0.6%) or a low phosphate diet (0.02%) for one week. **(E and H)** Plasma FGF23 measurements in 4-month-old *Furin;Pcsk5*$^{flox/flox}$ (n=4) and *Furin;Pcsk5*^{osb}*-/-* (n=4) 6 hours following an injection of vehicle and 300 U/kg of recombinant human erythropoietin (rhEPO): C-terminal FGF23 **(E)**, intact FGF23 **(F)**, percentage (%) of intact over C-terminal FGF23 **(G)** and cleaved FGF23 levels **(H)**, calculated as (C-terminal FGF23) - (intact FGF23). Results represent the mean ± SEM. *$P < 0.05$ and ***$P < 0.001$, by 2-way ANOVA with Bonferroni's multiple comparisons test, or by Student's t-test **(A and B)**.

371

372 mice genotype (Figure 6G-H). Altogether, these results show that FGF23 is still efficiently

373 processed *in vivo* even when both furin and PC5 were inactivated in osteoblasts and

374 osteocytes.

375

376

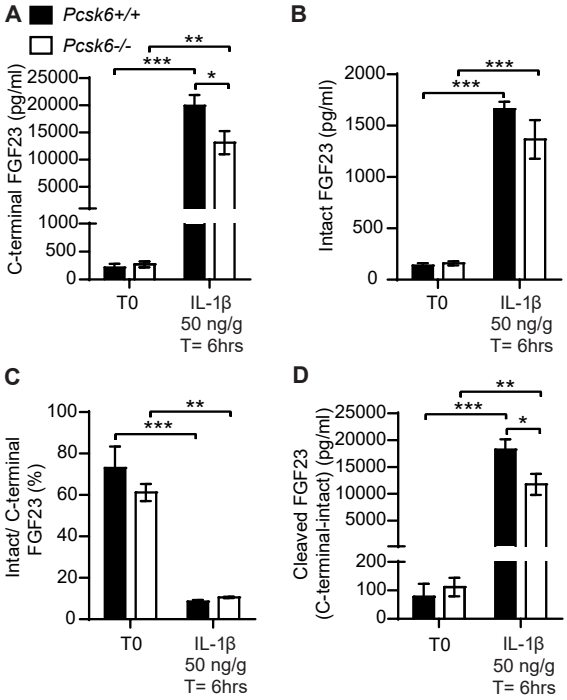

377 **Figure 7: PACE4 inactivation in mice does not**
378 **impair FGF23 processing.** Plasma FGF23
379 measurements in 4-month-old *Pcsk6* +/+ (n=4) and
380 *Pcsk6* -/- (n=4) male mice before (T0) and 6 hours
381 following the injection of 50 ng/g of IL-1β: C-terminal
382 FGF23 **(A)**, intact FGF23 **(B)**, percentage (%) of
383 intact over C-terminal FGF23 **(C)**, and cleaved
384 FGF23 levels **(D)**, calculated as (C-terminal FGF23)
385 - (intact FGF23). Results represent the mean ± SEM.
386 **P* < 0.05 and ****P* < 0.001, by 2-way ANOVA with
387 Bonferroni's multiple comparisons test.

388

389

390

391

392

393 **Whole body PACE4 deletion does not impair FGF23 processing under**

394 **physiological conditions or following IL-1β injections**

395 Combined inactivation of furin and PC5 failed to inhibit FGF23 processing in mice,

396 suggesting the potential involvement of at least one other enzyme in the regulation of

397 FGF23 *in vivo*. PACE4 can cleave FGF23 *in vitro* (Figure 5B) and is strongly expressed

398 in mouse osteoblasts [22]. We therefore next assessed FGF23 processing in PACE4

399 deficient mice (*Pcsk6-/-*) under physiological conditions and in response to IL-1β. When

400 fed a standard chow diet, *Pcsk6-/-* mice showed normal total (C-terminal) and intact

401 FGF23 plasma level compared to wild type littermates. However, 6h following a single IL-
402 1β (50ng/g) injection, these mice displayed a significant decrease in total (C-terminal)
403 FGF23 while intact FGF23 was not significantly changed (Figure 7A and 7B). The ratio of
404 intact over C-terminal FGF23 was equally decreased following IL-1β treatment in wild
405 type and *Pcsk6-/-* mice. Processed FGF23 was robustly increased by the same treatment
406 regardless of the genotype, although PACE4 deficient mice did displayed a significant
407 30% reduction compared to wild type mice (Figure 7C-D). Altogether, these results show
408 that PACE4 may partially contribute to FGF23 expression or secretion *in vivo* in response
409 to IL-1β. Yet, FGF23 is still processed in absence of PACE4, suggesting the redundant
410 action of other PCs.
411
412

413 **DISCUSSION**

414

415 More than 20 years ago, mutations in a putative proprotein convertase (PC) target
416 sequence within human FGF23 were found to cause ADHR in humans. Yet, the identity
417 of the specific PC(s) involved in FGF23 cleavage *in vivo* remained elusive. Taking
418 advantage of floxed alleles of *Furin* and *Psck5*, we generated mice lacking furin and/or
419 PC5 specifically in the osteoblasts and osteocytes lineage and assessed the role of these
420 two enzymes in regulating FGF23 processing *in vivo*. We provide evidence suggesting
421 that furin, but not PC5, partially regulates FGF23 processing *in vivo* under normal
422 conditions. We also exposed the mice to different challenges previously shown to regulate
423 FGF23 expression and its processing and show that FGF23 cleavage is largely mediated
424 by furin under conditions of iron deficiency. The requirement of furin for FGF23 processing
425 appears to be context or cell-type dependent, since FGF23 is still properly cleaved
426 following rhEPO or IL-1β injection when furin is inactivated alone or in combination with
427 PC5. Our results therefore suggest that additional peptidases may redundantly cleave
428 FGF23 *in vivo*.

429

430 When mice were fed standard chow diet, the modest increase in circulating intact FGF23
431 in *Furin*^{osb}*-/-* mice was not sufficient to cause hypophosphatemia and osteomalacia. This
432 result is consistent with the observation that ADHR patients show variable age of onset
433 and penetrance of the disease [35]. Since iron deficiency was shown to positively correlate
434 with FGF23 circulating levels in ADHR patient and to induce hypophosphatemia and
435 osteomalacia in mice carrying an AHDR mutation [14,15], we induced iron deficiency in

436 control and furin deficient mice. Under these conditions, furin deficient mice did not
437 develop hypophosphatemia and in fact displayed higher serum phosphate level despite
438 a near complete impairment of FGF23 cleavage. These observations suggest that
439 although furin may be important for the cleavage of FGF23 in osteocytes in the context
440 of iron deficiency, it may also be involved in the regulation of phosphate metabolism
441 through FGF23-independent mechanism(s).
442
443 The results obtained in the context of iron deficiency raised the question whether under
444 normal conditions FGF23 is redundantly cleaved by another enzyme that is
445 downregulated in osteocytes following iron deficiency. To clarify whether FGF23 cleavage
446 by furin is context specific, we injected controls and furin deficient mice with rhEPO or IL-
447 1β. These two circulating factors are produced in response to anemia and inflammation
448 respectively [16,36], and were shown to induce FGF23 secretion in bone and bone marrow
449 cells in rodents [16-19,26,27]. Carboplatin-mediated ablation of bone marrow hematopoietic
450 cells in mice suggest that osteoblasts and osteocytes may contribute to ~60% of the
451 increase in circulating FGF23 in response to rhEPO injections [26]. Herein, despite a strong
452 increase in circulating total (C-terminal) FGF23 level following rhEPO or IL-1β injection,
453 *Furin^{osb}-/-* mice did not show a concurrent increase in intact FGF23 suggesting cleavage
454 by one or several other PC(s) in osteocytes, or that cleaved FGF23 originates mainly from
455 bone marrow hematopoietic cells in this context. To address this second possibility, we
456 generated mice deficient in furin in osteoblast-derived cells and/or in all hematopoietic
457 cells. Surprisingly, our data shows that in these two cellular compartments, furin is
458 dispensable for FGF23 cleavage following the injection of rhEPO. These results provide

459 additional credence to the notion that furin is not the only peptidase involved in FGF23
460 processing *in vivo*.
461
462 We previously showed that PC5 (*Pcsk5*), PACE4 (*Pcsk6*) and PC7 (*Pcsk7*) are expressed
463 in differentiated osteoblasts [22]. These PCs also target the minimal consensus cleavage
464 site (i.e., RXXR) recognized by furin [37], suggesting that these PCs may also cleave
465 FGF23. We show herein that a mammalian cell line, furin, but also PC5, PACE4 and PC7
466 can process FGF23. However, inactivation of *Pcsk5* specifically in osteoblasts and
467 osteocytes did not impact intact FGF23 level and serum phosphate concentrations. In
468 addition, mice deficient in both furin and PC5 in the osteoblast lineage are comparable to
469 furin deficient mice in terms of FGF23 circulating level under physiological conditions and
470 following rhEPO injection, suggesting that PC5 does not compensate for furin absence *in*
471 *vivo*. Finally, even though PACE4 is highly expressed in differentiated osteoblasts [22] and
472 cleaves FGF23 in mammalian cells, *Pcsk6* inactivation in mice only reduced FGF23
473 production following IL-1β injection and did not impact its cleavage.
474
475 Altogether, these findings provide genetic evidence that furin in osteoblasts and
476 osteocytes is only partially responsible for FGF23 processing *in vivo*. Our data also
477 showed that FGF23 cleavage is differentially regulated depending on the physiological
478 context. Under conditions of iron deficiency furin is responsible for this process, while
479 following single injection of rhEPO or IL-1β, additional proteases may be involved in
480 FGF23 processing. Alternately, the increase in cleaved FGF23 following rhEPO and IL-
481 1β injection could originate from non-osteoblastic cells such as bone marrow

482 hematopoietic cells and involve multiple proteases including or not furin. Our study also
483 excluded PC5 and PACE4 as major FGF23 processing enzymes *in vivo.* In conclusion,
484 additional studies are required to determine precisely which enzyme(s) are involved in
485 FGF23 cleavage *in vivo* and how furin regulates phosphate metabolism independently of
486 FGF23.

487 **MATERIALS AND METHODS**

488

489 ***Mice and diets***

490 *Furin*$^{flox/flox}$ and *Pcsk5*$^{flox/flox}$ mice were generated by introducing loxP site flanking exon 2
491 of furin gene and exon 1 of Pcsk5 gene as described previously [38,39]. To generate
492 conditional knockout of furin (*Furin*^{osb}*-/-*) or PC5 (*Pcsk5*^{osb}*-/-*) in osteoblasts and
493 osteocytes, *Furin*$^{flox/flox}$ and *Pcsk5*$^{flox/flox}$ were crossed with OCN-Cre transgenic mice [22],
494 which express the Cre-recombinase under the control of human osteocalcin promoter [21].
495 *Furin;Pcsk5*^{osb}*-/-* mice are deficient in both *Furin* and *Pcsk5* in osteoblasts/osteocytes and
496 were generated by breeding *Furin*^{osb}*-/-* and *Pcsk5*$^{flox/flox}$ mice. *Furin*^{BM}*-/-* and *Furin*$^{osb;BM}$*-/-*
497 mice were generated by breeding *Furin*^{osb}*-/-* mice with *Furin*$^{flox/+}$*;Vav-iCre* mice. The Vav-
498 iCre expresses the Cre recombinase under the control of the *Vav* promoter, allowing the
499 efficient deletion of furin in fetal and adult hematopoietic stem cells (HSC) [29]. *Pcsk6-/-*
500 mice were provided by Dr. Robert Day (Université de Sherbrooke), these mice were
501 generated as described previously [40]. All mice were backcrossed at least 10 time with the
502 C57BL/6J genetic background, they were maintained at the IRCM pathogen free animal
503 facility on 12h light/dark cycle and fed a normal chow diet. In all experiments, unless
504 otherwise indicated, female mice were used.

505

506 In some indicated experiments mice were fed synthetic diet to induce iron or phosphate
507 deficiency. To induce iron deficiency, after weaning at 21 days old, mice were fed either
508 with normal chow diet or an iron deficient diet (Research diet, AIN-76A modified rodent
509 diet, D09070102i) for 14 weeks in combination with bleeding equivalent to one blood

510 capillary (70 μl) every two weeks. To induce phosphate deficiency, mice were fed for 5
511 days a normal phosphate diet (Envigo custom diet TD. 98243, 0.6% phosphorus), then
512 divided to two groups. The first group was maintained for one more week on 0.6% PI diet
513 while the second group was fed a phosphate deficient diet (Envigo custom diet, TD.
514 86128, 0.02% phosphorus). In other experiments, mice fed a normal chow diet were
515 injected with vehicle (saline or PBS), 300U/kg or 3000U/kg of recombinant human
516 erythropoietin (EPREX, Janssen-Cilag) or 50ng/g IL-1β (STEMCELL Technologies).
517

518 ***Serum biochemistry***

519 Intact and C-terminal FGF23 measurements were performed on EDTA plasma collected
520 from mice under fed conditions using ELISA assay specific for mouse intact or C-terminal
521 FGF23 (Quidel, cat#: 60-6800 and cat#: 60-6300). Since C-terminal FGF23 ELISA
522 detects both intact and processed FGF23, it reflects the total concentration of FGF23 in
523 the circulation. We also calculated the level of cleaved FGF23 by subtracting intact from
524 C-terminal values. At end of experiments, mice were anesthetized, and serum was
525 collected by heart puncture. Serum phosphate level was determined using a phosphorus
526 assay kit (Sekisui Diagnostic, cat#:117-30). For urine phosphate measurements, urine
527 was collected in the morning for 3 consecutive days and phosphate level was normalized
528 to creatinine measured using creatinine assay (Quidel, cat#: 8009).
529

530 ***RNA extraction***

531 Liver, kidney and bone marrow RNA was extracted using the standard protocol previously
532 described by Chomczynski *et al* [41], while bone RNA was extracted using Trizol reagent

533 (Thermo Fisher). cDNA was generated by RNA reverse transcription using M-MLV
534 Reverse Transcriptase (Thermo Fisher). Quantitative real-time PCR (qPCR) was
535 performed using specific primers (Key Resources Table Appendix) and SYBR Green
536 qPCR Master Mix (BiMake). Expression levels were normalized to *Actb* expression levels.
537

538 ***Von Kossa/ Van Gieson staining***

539 Mouse skeletons were collected and fixed in 10% formalin for 24 hours and in 70%
540 ethanol for at least an additional 24 hours. Lumbar vertebrae were collected and
541 dehydrated by gradual increase of ethanol percentage. Vertebrae were then embedded
542 in methyl methacrylate resin as described previously [42]. Vertebrae were sectioned at 7-
543 µm sections and stained with Von kossa/Van Gieson and images were analyzed using
544 the Osteomeasure analysis system (Osteometrics, Atlanta, GA).
545

546 ***FGF23 processing in cell culture***

547 The cDNAs coding for human furin, PC7, and PACE4, and mouse PC5A and PC5B were
548 cloned into the pIRES2-EGFP vector [43], while the cDNA of hFGF23 was cloned in
549 pIRES2-EGFP-V5. CHO-K1 and furin-deficient CHO-FD11 cells were cultured at 37 °C
550 and 5% CO_2 in Ham's F-12 medium supplemented with 10% (v/v) FBS [44] and transfected
551 with 3 µg of plasmid following the standard protocol for Lipofectamine 2000 (Thermo
552 Fisher). For the PCs inhibition, CHO-K1 cells were transfected with cDNAs encoding for
553 hFGF23-V5 and PCs in the ratio of 5:1 and 24 hours later pretreated for 5 hours with Dec-
554 RVKR-CMK (50 µM; Tocris) or D6R (20 µM; Calbiochem) followed by 22 hours of
555 treatment in serum free media. Cells supernatant was then collected in the presence of

556 1x complete protease inhibitor cocktail (Roche) and FGF23 processing was analyzed by
557 SDS-PAGE (15% Tris-glycine) followed by western blot using V5 antibody (Thermo
558 Fisher).
559
560 ***Statistics***
561 Statistical analyses were performed using GraphPad Prism software version 7.03.
562 Results are shown as the mean ± SEM. Unpaired, 2-tailed Student's *t* test was used for
563 single measurements or comparison between two groups, while 1-way or 2-way ANOVA
564 followed by Bonferroni's post-test were used for comparison of more than 2 groups.
565 A *P* value of less than 0.05 was considered statistically significant. All experiments were
566 performed at least on 3 independent animals. Before starting each *in vivo* experiment, the
567 mice were randomized into experimental groups with similar average body weight.
568
569

570 **ACKNOWLEDGEMENTS**

571 We thank Dr. R. Day for providing *Pcsk6*$^{-/-}$ mice, Dr. T. Clemens for sharing the hOC-Cre
572 mice and Dr. T. Möröy for the iVav-Cre strain. This work was supported by funding from
573 the Canada Research Chair program (M.F.) and the Natural Sciences and Engineering
574 Research Council of Canada (RGPIN-2016-05213, to MF) and a CIHR Foundation grant
575 (# 148363 to NGS). OAR received scholarships from IRCM and FRQS.

576

577 **CONFLICTS OF INTERESTS**

578 O.A.R., D.S.R., R.E., J.W.M.C., N.G.S., and M.F. have nothing to declare.
579

580

581 **REFERENCES**

582

583 1 Meyer, R. A., Jr., Meyer, M. H. & Gray, R. W. Parabiosis suggests a humoral factor
584 is involved in X-linked hypophosphatemia in mice. *J Bone Miner Res* **4**, 493-500,
585 doi:10.1002/jbmr.5650040407 (1989).

586 2 Miyauchi, A., Fukase, M., Tsutsumi, M. & Fujita, T. Hemangiopericytoma-induced
587 osteomalacia: tumor transplantation in nude mice causes hypophosphatemia and
588 tumor extracts inhibit renal 25-hydroxyvitamin D 1-hydroxylase activity. *J Clin*
589 *Endocrinol Metab* **67**, 46-53, doi:10.1210/jcem-67-1-46 (1988).

590 3 Urakawa, I. *et al.* Klotho converts canonical FGF receptor into a specific receptor
591 for FGF23. *Nature* **444**, 770-774, doi:10.1038/nature05315 (2006).

592 4 Larsson, T. *et al.* Transgenic mice expressing fibroblast growth factor 23 under the
593 control of the alpha1(I) collagen promoter exhibit growth retardation, osteomalacia,
594 and disturbed phosphate homeostasis. *Endocrinology* **145**, 3087-3094,
595 doi:10.1210/en.2003-1768 (2004).

596 5 Shimada, T. *et al.* FGF-23 is a potent regulator of vitamin D metabolism and
597 phosphate homeostasis. *J Bone Miner Res* **19**, 429-435,
598 doi:10.1359/JBMR.0301264 (2004).

599 6 Shimada, T. *et al.* Targeted ablation of Fgf23 demonstrates an essential
600 physiological role of FGF23 in phosphate and vitamin D metabolism. *J Clin Invest*
601 **113**, 561-568, doi:10.1172/JCI19081 (2004).

602 7 Shimada, T. *et al.* FGF-23 transgenic mice demonstrate hypophosphatemic rickets
603 with reduced expression of sodium phosphate cotransporter type IIa. *Biochem*
604 *Biophys Res Commun* **314**, 409-414, doi:10.1016/j.bbrc.2003.12.102 (2004).

605 8 Benet-Pages, A., Orlik, P., Strom, T. M. & Lorenz-Depiereux, B. An FGF23
606 missense mutation causes familial tumoral calcinosis with hyperphosphatemia.
607 *Hum Mol Genet* **14**, 385-390, doi:10.1093/hmg/ddi034 (2005).

608 9 Ichikawa, S. *et al.* Genetic rescue of glycosylation-deficient Fgf23 in the Galnt3
609 knockout mouse. *Endocrinology* **155**, 3891-3898, doi:10.1210/en.2014-1199
610 (2014).

611 10 Topaz, O. *et al.* Mutations in GALNT3, encoding a protein involved in O-linked
612 glycosylation, cause familial tumoral calcinosis. *Nat Genet* **36**, 579-581,
613 doi:10.1038/ng1358 (2004).

614 11 Tagliabracci, V. S. *et al.* Dynamic regulation of FGF23 by Fam20C
615 phosphorylation, GalNAc-T3 glycosylation, and furin proteolysis. *Proc Natl Acad*
616 *Sci U S A* **111**, 5520-5525, doi:10.1073/pnas.1402218111 (2014).

617 12 Consortium, A. Autosomal dominant hypophosphataemic rickets is associated with
618 mutations in FGF23. *Nat Genet* **26**, 345-348, doi:10.1038/81664 (2000).

619 13 Nesbitt, T., Coffman, T. M., Griffiths, R. & Drezner, M. K. Crosstransplantation of
620 kidneys in normal and Hyp mice. Evidence that the Hyp mouse phenotype is

621 unrelated to an intrinsic renal defect. *J Clin Invest* **89**, 1453-1459,
622 doi:10.1172/JCI115735 (1992).

623 14 Imel, E. A. *et al.* Iron modifies plasma FGF23 differently in autosomal dominant
624 hypophosphatemic rickets and healthy humans. *J Clin Endocrinol Metab* **96**, 3541-
625 3549, doi:10.1210/jc.2011-1239 (2011).

626 15 Farrow, E. G. *et al.* Iron deficiency drives an autosomal dominant
627 hypophosphatemic rickets (ADHR) phenotype in fibroblast growth factor-23
628 (Fgf23) knock-in mice. *Proc Natl Acad Sci U S A* **108**, E1146-1155,
629 doi:10.1073/pnas.1110905108 (2011).

630 16 David, V. *et al.* Inflammation and functional iron deficiency regulate fibroblast
631 growth factor 23 production. *Kidney Int* **89**, 135-146, doi:10.1038/ki.2015.290
632 (2016).

633 17 Hanudel, M. R. *et al.* Effects of erythropoietin on fibroblast growth factor 23 in mice
634 and humans. *Nephrol Dial Transplant*, doi:10.1093/ndt/gfy189 (2018).

635 18 Flamme, I., Ellinghaus, P., Urrego, D. & Kruger, T. FGF23 expression in rodents
636 is directly induced via erythropoietin after inhibition of hypoxia inducible factor
637 proline hydroxylase. *PLoS One* **12**, e0186979, doi:10.1371/journal.pone.0186979
638 (2017).

639 19 Daryadel, A. *et al.* Erythropoietin stimulates fibroblast growth factor 23 (FGF23) in
640 mice and men. *Pflugers Arch* **470**, 1569-1582, doi:10.1007/s00424-018-2171-7
641 (2018).

642 20 Yamamoto, H. *et al.* Posttranslational processing of FGF23 in osteocytes during
643 the osteoblast to osteocyte transition. *Bone* **84**, 120-130,
644 doi:10.1016/j.bone.2015.12.055 (2016).

645 21 Zhang, M. *et al.* Osteoblast-specific knockout of the insulin-like growth factor (IGF)
646 receptor gene reveals an essential role of IGF signaling in bone matrix
647 mineralization. *J Biol Chem* **277**, 44005-44012 (2002).

648 22 Al Rifai, O. *et al.* Proprotein convertase furin regulates osteocalcin and bone
649 endocrine function. *J Clin Invest* **127**, 4104-4117, doi:10.1172/JCI93437 (2017).

650 23 Bon, N. *et al.* Phosphate-dependent FGF23 secretion is modulated by
651 PiT2/Slc20a2. *Mol Metab* **11**, 197-204, doi:10.1016/j.molmet.2018.02.007 (2018).

652 24 Yu, X., Sabbagh, Y., Davis, S. I., Demay, M. B. & White, K. E. Genetic dissection
653 of phosphate- and vitamin D-mediated regulation of circulating Fgf23
654 concentrations. *Bone* **36**, 971-977, doi:10.1016/j.bone.2005.03.002 (2005).

655 25 Perwad, F. *et al.* Dietary and serum phosphorus regulate fibroblast growth factor
656 23 expression and 1,25-dihydroxyvitamin D metabolism in mice. *Endocrinology*
657 **146**, 5358-5364, doi:10.1210/en.2005-0777 (2005).

658 26 Clinkenbeard, E. L. *et al.* Erythropoietin stimulates murine and human fibroblast
659 growth factor-23, revealing novel roles for bone and bone marrow. *Haematologica*
660 **102**, e427-e430, doi:10.3324/haematol.2017.167882 (2017).

661 27 Toro, L. *et al.* Erythropoietin induces bone marrow and plasma fibroblast growth
662 factor 23 during acute kidney injury. *Kidney Int* **93**, 1131-1141,
663 doi:10.1016/j.kint.2017.11.018 (2018).

664 28 Clinkenbeard, E. L. *et al.* Conditional Deletion of Murine Fgf23: Interruption of the
665 Normal Skeletal Responses to Phosphate Challenge and Rescue of Genetic
666 Hypophosphatemia. *J Bone Miner Res* **31**, 1247-1257, doi:10.1002/jbmr.2792
667 (2016).

668 29 de Boer, J. *et al.* Transgenic mice with hematopoietic and lymphoid specific
669 expression of Cre. *European journal of immunology* **33**, 314-325,
670 doi:10.1002/immu.200310005 (2003).

671 30 Pesu, M. *et al.* T-cell-expressed proprotein convertase furin is essential for
672 maintenance of peripheral immune tolerance. *Nature* **455**, 246-250 (2008).

673 31 Susan-Resiga, D. *et al.* Furin is the major processing enzyme of the cardiac-
674 specific growth factor bone morphogenetic protein 10. *J Biol Chem* **286**, 22785-
675 22794, doi:10.1074/jbc.M111.233577 (2011).

676 32 Susan-Resiga, D. *et al.* Furin Is the Major Processing Enzyme of the Cardiac-
677 specific Growth Factor Bone Morphogenetic Protein 10. *J Biol. Chem.* **286**, 22785-
678 22794 (2011).

679 33 Seidah, N. G. & Prat, A. The biology and therapeutic targeting of the proprotein
680 convertases. *Nat Rev Drug Discov.* **11**, 367-383 (2012).

681 34 Essalmani, R. *et al.* In vivo functions of the proprotein convertase PC5/6 during
682 mouse development: Gdf11 is a likely substrate. *Proc. Natl. Acad. Sci. U. S. A.*
683 **105**, 5750-5755 (2008).

684 35 Imel, E. A., Hui, S. L. & Econs, M. J. FGF23 concentrations vary with disease
685 status in autosomal dominant hypophosphatemic rickets. *J Bone Miner Res* **22**,
686 520-526, doi:10.1359/jbmr.070107 (2007).

687 36 Jelkmann, W. Regulation of erythropoietin production. *J Physiol* **589**, 1251-1258,
688 doi:10.1113/jphysiol.2010.195057 (2011).

689 37 Seidah, N. G. & Prat, A. The biology and therapeutic targeting of the proprotein
690 convertases. *Nature reviews. Drug discovery* **11**, 367-383 (2012).

691 38 Essalmani, R. *et al.* In vivo functions of the proprotein convertase PC5/6 during
692 mouse development: Gdf11 is a likely substrate. *Proceedings of the National*
693 *Academy of Sciences of the United States of America* **105**, 5750-5755,
694 doi:10.1073/pnas.0709428105 (2008).

695 39 Roebroek, A. J. *et al.* Limited redundancy of the proprotein convertase furin in
696 mouse liver. *J Biol Chem* **279**, 53442-53450, doi:10.1074/jbc.M407152200 (2004).

697 40 Constam, D. B. & Robertson, E. J. SPC4/PACE4 regulates a TGFbeta signaling
698 network during axis formation. *Genes & development* **14**, 1146-1155 (2000).

699 41 Chomczynski, P. & Sacchi, N. The single-step method of RNA isolation by acid
700 guanidinium thiocyanate-phenol-chloroform extraction: twenty-something years
701 on. *Nature protocols* **1**, 581-585, doi:10.1038/nprot.2006.83 (2006).

702 42 Chappard, D., Palle, S., Alexandre, C., Vico, L. & Riffat, G. Bone embedding in
703 pure methyl methacrylate at low temperature preserves enzyme activities. *Acta*
704 *Histochem* **81**, 183-190 (1987).

705 43 Bergeron, E. *et al.* Implication of proprotein convertases in the processing and
706 spread of severe acute respiratory syndrome coronavirus. *Biochem Biophys Res*
707 *Commun* **326**, 554-563, doi:10.1016/j.bbrc.2004.11.063 (2005).

708 44 Gordon, V. M., Rehemtulla, A. & Leppla, S. H. A role for PACE4 in the proteolytic
709 activation of anthrax toxin protective antigen. *Infection and immunity* **65**, 3370-
710 3375, doi:10.1128/IAI.65.8.3370-3375.1997 (1997).

711

712

713 **FIGURES LEGENDS**

714

715 **Figure 1: Increased FGF23 level and reduced phosphate excretion in *Furin^{osb}-/-***
716 **mice.** FGF23 and phosphate levels in in 4-month-old *Furin$^{flox/flox}$* (n=6) and *Furin^{osb}-/-*
717 (n=6) mice fed on normal chow diet **(A-D)**. Intact FGF23 levels in plasma **(A)**. FGF23
718 target genes expression in kidney **(B)**. Serum phosphate level **(C)**. Von Kossa / van
719 Gieson staining on vertebrae sections **(D)**. FGF23 and phosphate parameters in 6-
720 months-old *Furin$^{flox/flox}$* (n=6) and *Furin^{osb}-/-* (n=6-7) mice fed a normal phosphate diet
721 (0.6%) or a low phosphate diet (0.02%) for one week **(E-N)**. Body weight **(E)**. Kidney
722 weight normalize to body weight **(F)**. Serum phosphate levels **(G)**. Plasma level of C-
723 terminal FGF23 **(H)**, intact FGF23 **(I)**, percentage (%) of intact over C-terminal FGF23 **(J)**
724 and cleaved FGF23 levels **(K)** calculated as (C-terminal FGF23) - (intact FGF23).
725 Expression level in kidney of the sodium phosphate cotransporter *Slc34a1* **(L)** and
726 *Slc34a3* **(M). (N)** Urine phosphate measurements normalized to creatinine. Results
727 represent the mean ± SEM. *P < 0.05, **P < 0.01, and ***P < 0.001, by 2-way ANOVA
728 with Bonferroni's multiple comparisons test or by Student's t-test (A, C, G, H, K, and M)
729 #: P<0.05; # #: P<0.01, # # #: P<0.001 &: 0.05<P<0.1.

730

731 **Figure 2: Impaired FGF23 processing in *Furin^{osb}-/-* mice following iron restriction.**
732 *Furin$^{flox/flox}$* (n=3-5) and *Furin^{osb}-/-* (n=7-8) 21-day-old mice were fed normal chow diet (ND)
733 or a low iron diet (LI) for 14 weeks. **(A)** Body weight growth curve presented as percentage
734 of initial body weight. **(B-C)** Expression of iron-regulated genes in liver. Hepcidin (*Hamp*)
735 expression **(B)**. Transferrin receptor (*Tfrc*) expression **(C). (D)** *Fgf23* expression in long
736 bone. **(E-H**) Plasma level of C-terminal FGF23 **(E)**, intact FGF23 **(F)**, percentage (%) of

737 intact over C-terminal FGF23 **(G)** and cleaved FGF23 levels **(H)**, calculated as (C-terminal
738 FGF23) - (intact FGF23). **(I)** Serum phosphate levels. Results represent the mean ± SEM.
739 *P < 0.05, **P < 0.01, and ***P < 0.001, by 2-way ANOVA with Bonferroni's multiple
740 comparisons test or by Student's t-test (D and E) #: P<0.05; # #: P<0.01, # # #: P<0.001
741 &: 0.05<P<0.1.
742
743 **Figure 3: FGF23 is normally processed following erythropoietin and IL-1β injection**
744 **in *Furin^{osb}*-/- mice.** Genes expression in long bone **(A, B and E)** and bone marrow **(C, D**
745 **and F)** of 2-month-old C57BL/6J mice 6 hours following the injection of vehicle (n=4), 300
746 U/kg (n=4) or 3000 U/kg (n=4) of recombinant human erythropoietin (rhEPO).
747 Erythropoietin receptor (*Epor*) **(A and C)**, erythroferrone (*Erfe*) **(B and D)** and FGF23
748 (*Fgf23*) **(C and F)**. **(G-J)** Plasma FGF23 measurements in 4-month-old *Furin$^{flox/flox}$* (n=3)
749 and *Furin^{osb}*-/- (n=3) mice 6 hours following the injection of vehicle, 300 U/kg or 3000 U/kg
750 of rhEPO. C-terminal FGF23 **(G)**, intact FGF23 **(H),** percentage (%) of intact over C-
751 terminal FGF23 **(I)** and cleaved FGF23 levels **(J)**, calculated as (C-terminal FGF23) -
752 (intact FGF23). **(K-N)** Plasma FGF23 measurements in 4-month-old *Furin$^{flox/flox}$* (n=4) and
753 *Furin^{osb}*-/- (n=4) mice before (T0) and 6 hours following the injection of 50 ng/g IL-1β
754 (T=6hrs). C-terminal FGF23 **(K)**, intact FGF23 **(L),** percentage (%) of intact over C-
755 terminal FGF23 **(M)** and cleaved FGF23 levels **(N)**. Results represent the mean ± SEM.
756 *P < 0.05, **P < 0.01, and ***P < 0.001, by 1-way ANOVA **(A-F)** or 2-way ANOVA **(G-N)**
757 with Bonferroni's multiple comparisons test, or by Student's t-test **(A and E)** #: P<0.05; #
758 #: P<0.01, # # #: P<0.001 &: 0.05<P<0.1.
759

760 **Figure 4: *Furin* inactivation in osteoblasts, osteocytes and hematopoietic cells did**
761 **not impair FGF23 processing following erythropoietin injection.** Plasma FGF23
762 measurements in 8-week-old *Furin*$^{flox/flox}$ (n=7), *Furin*^{osb}*-/-* (n=5), *Furin*^{osb}*-/-* (n=5) and
763 *Furin*$^{osb;BM}$*-/-* (n=6) mice 6 hours following injection of vehicle or 3000 U/kg of recombinant
764 human erythropoietin (rhEPO): C-terminal FGF23 **(A)**, intact FGF23 **(B)**, percentage (%)
765 of intact over C-terminal FGF23 **(C)** and cleaved FGF23 levels **(D)**, calculated as (C-
766 terminal FGF23) - (intact FGF23). Results represent the mean ± SEM. **P* < 0.05 and
767 ****P* < 0.001, by 2-way ANOVA with Bonferroni's multiple comparisons test.
768
769 **Figure 5: Multiple proprotein convertases can process FGF23 in mammalian cells.**
770 **(A)** Western blot analysis of the secretion media (SM) from CHO-K1 cells transfected with
771 V5 tagged human FGF23 (hFGF23-V5) and cultured in the absence (-) or presence (+)
772 of PC inhibitors, decanoyl-RVKR-CMK (RVKR) (50 μM) or hexa-D-arginine (D6R) (20
773 μM). **(B)** Western blot analysis of the secretion media (SM) from CHO furin-deficient FD11
774 cells co-transfected with V5 tagged human FGF23 (hFGF23-V5) and proprotein
775 convertase Furin, PC5A, PC5B, PACE4 or PC7. Intact and processed C-terminal (CT)
776 FGF23 forms are detected with V5 antibody.
777
778 **Figure 6: Genetic ablation of PC5 alone or in combination with Furin does not**
779 **impair FGF23 processing *in vivo*.** Plasma intact FGF23 **(A)** and serum phosphate
780 levels **(B)** in 4-month-old *Pcsk5*$^{flox/flox}$ (n=6) and *Pcsk5*^{osb}*-/-* (n=7) mice fed a normal chow
781 diet. **(C)** Von Kossa / van Gieson staining of vertebrae sections of *Pcsk5*$^{flox/flox}$ and
782 *Pcsk5*^{osb}*-/-*. **(D)** Plasma intact FGF23 in 6-month-old *Furin;Pcsk5*$^{flox/flox}$ (n=7-8) and

783 *Furin;Pcsk5*^{osb}*-/-* (n=8) fed a normal phosphate diet (0.6%) or a low phosphate diet
784 (0.02%) for one week. **(E and H)** Plasma FGF23 measurements in 4-month-old
785 *Furin;Pcsk5*$^{flox/flox}$ (n=4) and *Furin;Pcsk5*^{osb}*-/-* (n=4) 6 hours following an injection of
786 vehicle and 300 U/kg of recombinant human erythropoietin (rhEPO): C-terminal FGF23
787 **(E)**, intact FGF23 **(F)**, percentage (%) of intact over C-terminal FGF23 **(G)** and cleaved
788 FGF23 levels **(H)**, calculated as (C-terminal FGF23) - (intact FGF23). Results represent
789 the mean ± SEM. *$P < 0.05$ and ***$P < 0.001$, by 2-way ANOVA with Bonferroni's multiple
790 comparisons test, or by Student's t-test **(A and B)**.
791
792 **Figure 7: PACE4 inactivation in mice does not impair FGF23 processing.** Plasma
793 FGF23 measurements in 4-month-old *Pcsk6* +/+ (n=4) and *Pcsk6* -/- (n=4) male mice
794 before (T0) and 6 hours following the injection of 50 ng/g of IL-1β: C-terminal FGF23 **(A)**,
795 intact FGF23 **(B)**, percentage (%) of intact over C-terminal FGF23 **(C)**, and cleaved
796 FGF23 levels **(D)**, calculated as (C-terminal FGF23) - (intact FGF23). Results represent
797 the mean ± SEM. *$P < 0.05$ and ***$P < 0.001$, by 2-way ANOVA with Bonferroni's multiple
798 comparisons test.
799
800

Key Resources Table Appendix: Primers used				
Reagent type (species) or resource	**Designation**	**Source or reference**	**Identifiers**	**Additional information**
Sequence-based reagent	Actin beta- For	This paper	QPCR primer (amplify *Actb*, M. musculus)	GACCTCTAT GCCAACACAGT
Sequence-based reagent	Actin beta- Rev	This paper	QPCR primer (amplify *Actb*, M. musculus)	AGTACTTGC GCTCAGGAGGA
Sequence-based reagent	Slc34a1-Fw	This paper	QPCR primer (amplify *Slc34a1*, M. musculus)	GCATCCTACTGTGGTAC CCG
Sequence-based reagent	Slc34a1-Rv	This paper	QPCR primer (amplify *Slc34a1*, M. musculus)	CAGCAAACCAGCGGTA CTTG
Sequence-based reagent	Slc34a3-Fw	This paper	QPCR primer (amplify *Slc34a3*, M. musculus)	CCTTTGGACTTTCCCTG GCA
Sequence-based reagent	Slc34a3-Rv	This paper	QPCR primer (amplify *Slc34a3*, M. musculus)	GATGGTCGGTGTTGTT GCAG
Sequence-based reagent	Hamp-Fw	This paper	QPCR primer (amplify *Hamp*, M. musculus)	AGAGCTGCAGCCTTTG CAC
Sequence-based reagent	Hamp-Rv	This paper	QPCR primer (amplify *Hamp*, M. musculus)	GAGGTCAGGATGTGGC TCTA
Sequence-based reagent	Tfrc-Fw	This paper	QPCR primer (amplify *Tfrc*, M. musculus)	TAAATTCCCCGTTGTTG AGG
Sequence-based reagent	Tfrc-Rv	This paper	QPCR primer (amplify *Tfrc*, M. musculus)	CAGGACAGCTTCCTTC CATT
Sequence-based reagent	Cyp27b1-Fw	This paper	QPCR primer (amplify *Cyp27b1*, M. musculus)	GAAGCTGCGATGAGGA ACCA
Sequence-based reagent	Cyp27b1-Rv	This paper	QPCR primer (amplify *Cyp27b1*, M. musculus)	TTCCCCACTATGGACTG GACA
Sequence-based reagent	Cyp24a1-Fw	This paper	QPCR primer (amplify *Cyp24a1*, M. musculus)	CCCAGCGGCTAGAGAT CAAA
Sequence-based reagent	Cyp24a1-Rv	This paper	QPCR primer (amplify *Cyp24a1*, M. musculus)	TTTCTTTTGGAAGGCGC TGC

Sequence-based reagent	Fgf23-Fw	This paper	QPCR primer (amplify *Fgf23*, M. musculus)	CCGCTGCTGCATTTCTACAC
Sequence-based reagent	Fgf23-Rv	This paper	QPCR primer (amplify *Fgf23*, M. musculus)	CTTGAGCACGTTCAGTGGGT
Sequence-based reagent	Epor-Fw	This paper	QPCR primer (amplify *Epor*, M. musculus)	GGACACAAAGGGTGGAGGTC
Sequence-based reagent	Epor-Rv	This paper	QPCR primer (amplify *Epor*, M. musculus)	GCTCGAACAGCGAAGGTGTA
Sequence-based reagent	Erfe-Fw	This paper	QPCR primer (amplify *Erfe*, M. musculus)	GTTCCAGCTGTTGCTGAAAGG
Sequence-based reagent	Erfe-Rv	This paper	QPCR primer (amplify *Erfe*, M. musculus)	TACCCGAGGCTGGTGTAGTG

801